HHS Public Access

Author manuscript

Sci Transl Med. Author manuscript; available in PMC 2016 July 06.

Published in final edited form as:

Sci Transl Med. 2015 August 26; 7(302): 302ra136. doi:10.1126/scitranslmed.aac9459.

A DLL3-targeted antibody-drug conjugate eradicates high-grade pulmonary neuroendocrine tumor-initiating cells in vivo

Laura R. Saunders[1], **Alexander J. Bankovich**[1], **Wade C. Anderson**[1], **Monette A. Aujay**[1], **Sheila Bheddah**[1], **KristenAnn Black**[1], **Radhika Desai**[1], **Paul A. Escarpe**[1], **Johannes Hampl**[1], **Amy Laysang**[1], **David Liu**[1], **Javier Lopez-Molina**[1], **Milly Milton**[1], **Albert Park**[1], **Marybeth A. Pysz**[1], **Hui Shao**[1], **Brian Slingerland**[1], **Michael Torgov**[1,*], **Samuel A. Williams**[1], **Orit Foord**[1], **Philip Howard**[2], **Jacek Jassem**[3], **Andrzej Badzio**[3], **Piotr Czapiewski**[3], **David H. Harpole**[4], **Afshin Dowlati**[5], **Pierre P. Massion**[6], **William D. Travis**[7], **M. Catherine Pietanza**[7,8], **J. T. Poirier**[7,8], **Charles M. Rudin**[7], **Robert A. Stull**[1], and **Scott J. Dylla**[1,†]

[1]Stemcentrx Inc., South San Francisco, CA 94080, USA [2]Spirogen (a member of the AstraZeneca Group), London W2 6BD, UK [3]Medical University of Gdańsk, Gdańsk 82-300, Poland [4]Duke University Medical Cancer, Durham, NC 27710, USA [5]Case Western Reserve University and University Hospitals Seidman Cancer Center, Cleveland, OH 44106, USA [6]Thoracic Program,

[†]Corresponding author. scott.dylla@stemcentrx.com.
[*]Present address: ImaginAb Inc., Inglewood, CA 90301, USA.

SUPPLEMENTARY MATERIALS

www.sciencetranslationalmedicine.org/cgi/content/full/7/302/302ra136/DC1

Materials and Methods
Fig. S1. Elevated expression of *DLL3* mRNA in SCLC.
Fig. S2. Specificity of anti-DLL3 IHC antibody.
Fig. S3. DLL3 protein expression by IHC in representative samples from tissue microarrays.
Fig. S4. In vitro plasma stability of SC16LD6.5.
Fig. S5. Enumeration of cells with localization of human antibody in the late endosome.
Fig. S6. DLL3 knockdown confirmation by flow cytometry.
Fig. S7. In vivo efficacy of SC16LD6.5, naked SC16 antibody, and free toxin, D6.5.
Fig. S8. In vivo tolerability of SC16LD6.5.
Fig. S9. Elimination of TICs by SC16LD6.5.
Fig. S10. Off-target toxicities observed in nonhuman primates.
Table S1. DLL3 normal tissue expression.
Table S2. DLL3 microarray expression in PDX.
Table S3. Biacore affinity characterization of SC16 and SC16LD6.5 binding to human, cyno, and rat DLL3.
Table S4. LU64 TIC frequency determination.
Table S5. DLL3 whole transcriptome metrics (provided as an Excel file).

Author contributions: L.R.S. designed and executed experiments; collected, analyzed, and interpreted data; and wrote the manuscript. A.J.B., W.C.A., M.A.A., and J.H. designed and executed experiments; collected, analyzed, and interpreted data; and reviewed the manuscript. S.B. and J.L.-M. designed and executed experiments and collected, analyzed, and interpreted data. K.B., R.D., P.A.E., A.L., D.L., M.M., H.S., M.T., S.A.W., and O.F. designed and executed experiments. A.P. and M.A.P. analyzed and interpreted data, including statistical analyses. B.S., P.H., J.J., A.B., P.C., D.H.H., A.D., P.P.M., W.D.T., and M.C.P. coordinated and contributed specimens and molecules critical to this work. J.T.P. and C.M.R. analyzed and interpreted data, including statistical analyses, and contributed to the writing of the manuscript. R.A.S. and S.J.D. designed experiments, analyzed and interpreted data, and wrote the manuscript.

Competing interests: L.R.S., A.J.B., W.C.A., M.A.A., S.B., K.B., R.D., P.A.E., J.H., A.P., A.L., D.L., J.L.-M., M.M., M.A.P., H.S., M.T., S.A.W., O.F., R.A.S., B.S., and S.J.D. are shareholders in Stemcentrx Inc., a privately held and financed company.

The following issued and pending patent applications pertain to the results presented here: U.S. issued patent: 8,986,972; U.S. pending patent applications: 14/466,842, 14/466,941, 14/466,945, 14/466,948, 14/466,951, 14/733,874, and 14/742,576; PCT patent applications: PCT/US13/027391 and PCT/US14//017810.

Data and materials availability: Materials are available from Stemcentrx under a material transfer agreement.

Vanderbilt-Ingram Cancer Center, Tennessee Valley Healthcare Systems, Nashville Campus, Nashville, TN 37232, USA [7]Memorial Sloan Kettering Cancer Center, New York, NY 10065, USA [8]Weill Cornell Medical College, New York, NY 10065, USA

Abstract

The high-grade pulmonary neuroendocrine tumors, small cell lung cancer (SCLC) and large cell neuroendocrine carcinoma (LCNEC), remain among the most deadly malignancies. Therapies that effectively target and kill tumor-initiating cells (TICs) in these cancers should translate to improved patient survival. Patient-derived xenograft (PDX) tumors serve as excellent models to study tumor biology and characterize TICs. Increased expression of delta-like 3 (*DLL3*) was discovered in SCLC and LCNEC PDX tumors and confirmed in primary SCLC and LCNEC tumors. DLL3 protein is expressed on the surface of tumor cells but not in normal adult tissues. A DLL3-targeted antibody-drug conjugate (ADC), SC16LD6.5, comprised of a humanized anti-DLL3 monoclonal antibody conjugated to a DNA-damaging pyrrolobenzodiazepine (PBD) dimer toxin, induced durable tumor regression in vivo across multiple PDX models. Serial transplantation experiments executed with limiting dilutions of cells provided functional evidence confirming that the lack of tumor recurrence after SC16LD6.5 exposure resulted from effective targeting of DLL3-expressing TICs. In vivo efficacy correlated with DLL3 expression, and responses were observed in PDX models initiated from patients with both limited and extensive-stage disease and were independent of their sensitivity to standard-of-care chemotherapy regimens. SC16LD6.5 effectively targets and eradicates DLL3-expressing TICs in SCLC and LCNEC PDX tumors and is a promising first-in-class ADC for the treatment of high-grade pulmonary neuroendocrine tumors.

INTRODUCTION

High-grade pulmonary neuroendocrine tumors, which include small cell lung cancer (SCLC) and large cell neuroendocrine carcinoma (LCNEC), represent ~18% of primary lung neoplasms and predominantly develop in older patients with a history of smoking (1, 2). Both SCLC and LCNEC remain among the most deadly malignancies because no new therapeutic options have emerged for these indications in more than 30 years (3, 4). SCLC survival is measured in months, with a 5-year survival rate <5%. Prognosis is also poor but more variable for LCNEC (5, 6). SCLC is an aggressive disease that is commonly metastatic at the time of diagnosis and is rarely amenable to surgery. The standard of care (SOC) for patients with extensive-stage SCLC is chemotherapy with etoposide and a platinating agent such as cisplatin or carboplatin. For about one-third of patients with limited-stage disease, in which the tumor is confined to one hemithorax and may be targeted within a single radiation port, the same chemotherapy with concurrent radiotherapy defines SOC (4). Although SCLC tumors are exquisitely sensitive to chemotherapy, relapses generally occur shortly after cessation of SOC (1). The only widely approved second-line therapy, topotecan, provides a ~17% response rate, a median progression-free survival of 3 months, and an overall survival of less than 7 months (7). Although there is no clear treatment consensus for LCNEC, it is commonly treated similarly to SCLC. Given the poor prognosis and lack of treatment

options, it is desirable to identify new therapeutic targets and treatment modalities to improve patient outcomes.

Cellular heterogeneity is commonly observed within tumors, which contain distinct tumor cell subpopulations with differing morphology, genetic mutations, and capacity to proliferate and with inherent differential sensitivity to chemotherapeutic agents (8, 9). The mutagenic effects of cigarette smoke are reflected in the types of DNA mutations seen in SCLC tumors, and distinct chromosomal gains and losses can distinguish SCLC and LCNEC from other types of lung cancer (10, 11). Tumor-initiating cells (TICs) encompass both tumor progenitor cells and cancer stem cells, the latter of which can be distinguished from the former by their capacity for self-renewal and reconstitution of the original tumor heterogeneity in serial transplants (12). Low-passage patient-derived xenograft (PDX) tumor models better reflect human tumor cell heterogeneity than do conventional cell lines and xenografts and are useful for identifying potential targets associated with TICs and for assessing in vivo response to therapeutic agents (12–15).

SCLC TICs likely arise from normal pulmonary neuroendocrine cells (PNECs), the portion of the diffuse neuroendocrine system found in the respiratory epithelium. PNECs regulate branching morphogenesis and oxygen sensing and are abundant in the developing lung (16). Mouse models replicating the oncogenic mutations and tumor suppressor losses observed in patients have implicated PNECs, or a multipotential precursor that gives rise to PNECs, as the cell of origin for SCLC (17–19). Critical for PNEC development is the transcription factor achaete-scute homolog-1 (*ASCL1*; murine ortholog *Mash1*). *Mash1* expression in the developing mouse lung peaks at birth and declines in adulthood, and mice lacking *Mash1* die soon after birth because of lung defects (20–23). *ASCL1* is also important in neuroendocrine cell fate decisions and is highly expressed in classic SCLC and LCNEC tumors, where it acts to maintain neuroendocrine features (21). *ASCL1* expression correlates with the tumor-initiating capacity of SCLC tumors (24).

The Notch pathway has likewise been implicated in regulating neuroendocrine versus epithelial cell fate decisions in the developing lung (25). The mammalian Notch family ligands DLL1, DLL4, JAG1, and JAG2 each activate Notch receptor signaling in trans (26). In contrast, the related ligand delta-like 3 (DLL3) predominantly localizes to the Golgi apparatus and is unable to activate Notch signaling (27, 28). DLL3 shares only 36% homology with DLL1 and differs from other deltatype DSL (Delta/Serrate/LAG-2) proteins, DLL1 and DLL4, in both its reduced number of epidermal growth factor (EGF)–like repeats and spacing of the cysteine residues within its DSL domain, which is required for Notch binding (29). Normal tissue expression of DLL3 is highest in fetal brain, and DLL3 plays a key role in somitogenesis in the paraxial mesoderm (27, 28, 30–32). Although Notch pathway activation acts as an oncogenic stimulus in some tumor types (33), Notch activation in neuroendocrine tumors suppresses tumor growth (34). In the course of normal development, DLL3 inhibits both cis- and transacting Notch pathway activation by interacting with Notch and DLL1 and redirecting or retaining them to late endosomal/lysosomal compartments or the Golgi, respectively, thereby preventing their localization to the cell surface (27, 35). Moreover, DLL3 is one of several Notch ligands that appear to be direct downstream targets of ASCL1 (36, 37). Together, these observations suggest that

DLL3 might be associated with the neuroendocrine phenotype and contributes to neuroendocrine tumorigenesis.

We set out to explore heterogeneity in SCLC and LCNEC PDX by characterizing gene expression in TICs from these tumors. Whole transcriptome data from isolated populations of SCLC and LCNEC tumor cells showed *DLL3* expression to be increased relative to normal tissues, including normal lung. Further analysis showed that DLL3 protein was detectable at the surface of SCLC and LCNEC tumor cells, leading to the hypothesis that it could make a tractable therapeutic target for an antibody-drug conjugate (ADC) in these cancers (38). We developed an ADC to leverage the potent activity of the cell cycle–independent pyrrolobenzodiazepine (PBD) cytotoxin D6.5, with the expectation that it would selectively kill *DLL3*-expressing tumor cells and limit systemic toxicities. Here, we show that the DLL3-targeted ADC, SC16LD6.5, effectively targets and eradicates TICs in both SCLC and LCNEC PDX tumors.

RESULTS

Increased DLL3 expression in high-grade pulmonary neuroendocrine tumors

SCLC and LCNEC PDX tumors were previously established from transbronchial needle aspirates or tumor resections (14). Four SCLC and one LCNEC PDX were dissociated to single-cell suspensions, and tumor cells were isolated using fluorescence-activated cell sorting (FACS). Isolated subpopulations were transplanted to evaluate their tumorigenicity, and whole transcriptome sequencing was performed in parallel to identify differentially expressed genes. *DLL3* was identified as >100-fold overexpressed in SCLC and LCNEC PDX versus seven different normal vital organs, including the lung (table S1), and was increased in all populations of TICs (Fig. 1A).

To verify whole transcriptome data and expand analysis to additional samples, we performed quantitative reverse transcription polymerase chain reaction (qRT-PCR) in four primary SCLC tumor biopsy specimens matched to established PDX models, an additional 15 SCLC and 2 LCNEC PDX, and 26 normal human tissues. Elevated expression of *DLL3* mRNA was confirmed in these primary SCLC tumors and low-passage SCLC and LCNEC PDX tumors (Fig. 1B). Among normal tissues, mRNA expression was limited to the brain, esophagus, and pancreas, with the last two having 1000-fold lower levels than SCLC and LCNEC PDX tumors (table S1). Because *DLL3* is thought to be a transcriptional target of ASCL1 (36), its expression was also assessed and found to significantly correlate with *DLL3* expression in SCLC and LCNEC PDX (Fig. 1C; Pearson $r^2 = 0.66$, $P < 0.0001$). Previous studies have classified SCLC into two subtypes that can be discriminated by high expression of *ASCL1* (classic SCLC) or high expression of *NEUROD1* (variant SCLC) (39, 40). Consistent with their classification as variant SCLC, LU80 and LU100 had lower *ASCL1* and *DLL3* expression (Fig. 1C) but higher *NEUROD1* expression (Fig. 1D and fig. S1A). Notably, the cisplatin and etoposide (C/E) refractory PDX tumor model LU86 (14) had high *NEUROD1* and *DLL3* expression despite low *ASCL1* expression. Collectively, our data show high expression of *DLL3* in most of classic SCLC, with lower levels in variant SCLC.

To further expand our analysis of tumor and normal tissue specimens, we examined *DLL3* expression in whole transcriptome sequencing data sets from 29 primary SCLC biopsy specimens, 25 SCLC cell lines, and 25 normal lung biopsy specimens (11). This analysis confirmed our initial observations, revealing a ~35-fold elevation in *DLL3* mRNA in SCLC relative to normal lung (Fig. 1E). These SCLC tumor samples were compared to transcriptome data from normal tissues and other tumor types in The Cancer Genome Atlas data set, which further confirmed elevated *DLL3* expression in primary SCLC tumor samples, as well as low-grade glioma, glioblastoma, and melanoma (fig. S1B). Illumina BeadChip data from the Clinical Lung Cancer Genome Project (10) also showed *DLL3* elevation in primary SCLC tumor specimens compared to NSCLC (fig. S1C).

Finally, microarray gene expression analysis of 14 SCLC and 2 LCNEC PDX models revealed ~120-fold elevation in expression of *DLL3* mRNA compared to 12 normal tissues (Fig. 1F and tables S1 and S2). These observations were further confirmed by publically available microarray data sets from the Cancer Cell Line Encyclopedia (41), which show elevated *DLL3* mRNA expression specifically in SCLC cell lines (fig. S1D). Collectively, these expression data across numerous technical platforms and samples show that *DLL3* mRNA is overexpressed in primary SCLC tumors, SCLC PDX, conventional SCLC cell lines, and LCNEC PDX, whereas mRNA expression in normal tissues appears limited primarily to the brain.

Generation and characterization of DLL3-specific monoclonal antibodies

To assess protein expression and determine whether DLL3 is on the surface of tumor cells, anti-DLL3 antibodies were generated and characterized. In separate immunization campaigns, recombinant DLL3-Fc (Adipogen) or DLL3-His protein purified from supernatants of transfected CHOK1 (Chinese hamster ovary–K1) cells was used as an immunogen to produce mouse monoclonal antibodies that were confirmed to bind DLL3 by enzyme-linked immunosorbent assay (ELISA) and flow cytometry. Several antibodies binding to different DLL3 epitopes were humanized by CDR grafting of the murine variable regions onto the human immunoglobulin G1 (IgG1)/κ constant regions and were confirmed to maintain affinity for human, cynomolgus monkey (cyno), and rat DLL3 antigens. Data for a representative humanized monoclonal antibody, SC16, are shown in table S3. Cross-reactivity and equivalent SC16 binding to DLL3 from species relevant for toxicology studies were demonstrated using human embryonic kidney (HEK)–293T cells transduced and selected for expression of human, cyno, or rat DLL3, respectively. Flow cytometry confirmed that SC16 bound to each of these proteins on the surface of nonpermeabilized, engineered HEK-293T cells (Fig. 2A), establishing that DLL3 protein can localize to the cell surface and is not necessarily confined to the Golgi (27, 28). The specificity of SC16 for DLL3, and not its related family members DLL1 or DLL4, was demonstrated by ELISA (Fig. 2B). These studies establish that SC16 is specific for DLL3, that DLL3 can localize to the cell surface, and that the affinity of SC16 for human, cyno, or rat antigen is in the low nanomolar range and within threefold across species (table S3).

Surface expression of DLL3 in SCLC and LCNEC

To measure protein expression in tumor and tissue lysates, we developed a sandwich ELISA using two noncompeting DLL3 monoclonal antibodies. Analysis of total protein lysates from 28 normal tissues, 14 SCLC PDX, and 2 LCNEC PDX showed that DLL3 protein expression in normal tissues was below the limit of quantitation of 0.37 part per million (ppm; ng DLL3/mg total protein) in all tissues except the heart and adrenal gland (table S1), whereas an average of 3.7 ppm was detected in SCLC PDX tumors, along with very elevated expression in the two LCNEC PDXs evaluated (Fig. 2C). Notably, there was no DLL3 protein above the limit of detection in the brain, despite high mRNA expression. Furthermore, the SCLC PDXs that had lower mRNA expression (LU80 and LU100) were likewise found to have low levels of DLL3 protein (0.6 ppm and below the limit of detection, respectively).

To further explore protein expression and its cellular localization in SCLC and LCNEC tumors, we identified a DLL3-specific monoclonal antibody for immunohistochemistry (IHC) using formalin-fixed, paraffin-embedded samples (fig. S2). An initial assessment of two SCLC PDX (LU64 and LU149), one LCNEC PDX (LU37), and primary biopsy samples from SCLC and LCNEC patients demonstrated both membranous and cytoplasmic staining (Fig. 2D). This staining pattern is consistent with previous observations of localization for other Notch ligands and receptors (27, 28). The membrane localization of DLL3 staining was quantified in primary tumor specimens, using tissue microarrays encompassing 9 normal lung samples, 95 non-SCLC (82 adenocarcinoma and 13 squamous cell carcinoma), 57 LCNEC, and 187 SCLC tumor specimens. Surface DLL3 expression was quantified by converting the staining intensity (range, 0 to 3) and the percentage of cells with expression to an *H*-score (range, 0 to 300) (Fig. 2E and fig. S3). No normal lung specimen or lung squamous cell carcinoma tumor cells stained positively, whereas 37 of 57 LCNEC (65%), 120 of 167 treatment-naïve SCLC (72%), and 17 of 20 recurrent and treatment-refractory (R/R) SCLC (85%) exceeded an *H*-score of 100. Notably, 3 of 82 (3.7%) lung adenocarcinoma tumors had DLL3 expression, suggesting the presence of neuroendocrine components in these tumors (Fig. 2E). This is consistent with previous observations of ASCL1 expression and other neuroendocrine markers in ~10% of lung adenocarcinoma, exclusively in patients who smoked (42). We next explored DLL3 expression on the surface of cells from dissociated PDX tumors using flow cytometry and a PE-conjugated DLL3 antibody. Data from representative SCLC PDX (LU149) and LCNEC PDX (LU37) models show expression of DLL3 on the cell surface (Fig. 2F). Collectively, the above data show that elevated *DLL3* mRNA expression translates to detectable protein at the cell surface in SCLC and LCNEC tumors, but not normal tissue.

Internalization and toxin delivery by anti-DLL3 monoclonal antibodies

To evaluate whether anti-DLL3 antibodies can mediate internalization and delivery of a potent cytotoxin, we generated an ADC targeting DLL3, SC16LD6.5. SC16LD6.5 is comprised of the D6.5 PBD payload conjugated to cysteine residues on the SC16 antibody via a maleimide-containing linker with an eight-carbon polyethylene glycol spacer, cathepsin B–cleavable valine-alanine dipeptide, and self-immolating group (Fig. 3A), with a mean drug-to-antibody ratio of 2. Both SC16LD6.5 and unconjugated SC16 had comparable

affinity for human, cyno, and rat DLL3 (table S3). Additionally, SC16LD6.5 was incubated in human serum and shown to be stable in physiologically relevant conditions with minimal release of D6.5 over time (fig. S4).

To evaluate whether DLL3 was internalized after antibody or ADC engagement, we evaluated its intracellular trafficking using immunofluorescence colocalization analysis. Specifically, parental HEK-293T cells and cells overexpressing human DLL3 (HEK-293T.hDLL3) were infected with a baculovirus expressing a fluorescently labeled protein [stomatin-like protein-1 (SLP-1)] that localizes to late endosomes (43), a prelysosomal endocytic compartment with low pH and abundance of cathepsin B, which is responsible for efficient valine-alanine dipeptide cleavage (44, 45). Infected cells were then exposed to SC16, SC16LD6.5, an anti-hapten human IgG1 control antibody, or an IgG1 control ADC (IgG1LD6.5). Both unconjugated SC16 and SC16LD6.5 were internalized in HEK-293T.hDLL3 cells and were localized to the late endosomes, as indicated by the overlap of green and red color manifest as yellow/orange (Fig. 3B, left panel, and fig. S5). In contrast, no overlapping signal was detected in HEK-293T cells (fig. S5). Neither control antibody nor control ADC was internalized in HEK-293T.hDLL3 cells (Fig. 3B, right panel, and fig. S5). Finally, the number of cells showing localization of antibodies to late endosomes was enumerated, demonstrating that SC16 and SC16LD6.5 were specifically internalized and trafficked to late endosomes in cells expressing DLL3 (fig. S5).

To evaluate in vitro cytotoxicity, HEK-293T or HEK-293T.hDLL3 cells were incubated with increasing concentrations of the free drug D6.5, SC16, SC16LD6.5, or IgG1LD6.5, and cell viability was measured 4 days later. Exposure to D6.5 mediated equivalent killing of HEK-293T and HEK-293T.hDLL3 cells, and neither SC16 nor IgG1LD6.5 mediated any cell killing (Fig. 3, C and D). SC16LD6.5 mediated potent and specific killing of HEK-293T.hDLL3 cells in an antigen- and concentration-dependent manner, demonstrated by sixfold greater potency than D6.5 alone [EC_{50} (median effective concentration), 7.8 versus 46.9 pM; Fig. 3D]. We further evaluated cytotoxicity on LU64 SCLC tumor cells plated in vitro and found that SC16LD6.5 potently and specifically mediated cytotoxicity (EC_{50}, 8.3 pM), whereas D6.5 was unable to achieve cell killing at concentrations up to 500 pM (Fig. 3E). Collectively, these data demonstrate that SC16LD6.5 is internalized and mediates cytotoxicity in an antigen-dependent manner and that sufficient endogenous DLL3 is present in SCLC PDX tumor cells to mediate potent cell killing.

Finally, to validate the specificity of SC16LD6.5 for DLL3-expressing cells, dissociated LU37 LCNEC PDX tumor cells were transduced with a lentivirus expressing a *DLL3*-targeted short hairpin RNA (shRNA) and were cultured in vitro (LU37.D3hp). Successful knockdown of DLL3 expression in LU37.D3hp cells was confirmed by flow cytometry (fig. S6). Both LU37 and LU37.D3hp cells were exposed to varying concentrations of either SC16LD6.5 or IgG1LD6.5. Whereas LU37 cells were killed by SC16LD6.5 in a concentration-dependent manner (EC_{50}, 13.3 pM; Fig. 3F), LU37.D3hp cells were not (Fig. 3G), demonstrating that the cytotoxic activity of SC16LD6.5 is dependent on the presence of the DLL3 antigen on the cell surface.

Reduction of TICs by SC16LD6.5 in vivo

To evaluate the in vivo efficacy of SC16LD6.5, nonobese diabetic–severe combined immunodeficiency (NOD/SCID) mice were implanted with SCLC or LCNEC PDX tumor cells and were randomized into groups of five to eight mice once tumor volumes reached ~140 to 200 mm^3. Each group was treated intraperitoneally with three doses of SC16LD6.5 or IgG1LD6.5 (1 mg/kg) every 4 days (Q4D×3; Fig. 4, A to C). Separate cohorts of SCLC tumor–bearing mice were treated with vehicle or SOC chemotherapy consisting of cisplatin (5 mg/kg) and etoposide (8 mg/kg) (C/E) on the day of randomization, followed by etoposide on the subsequent 2 days. LCNEC tumor–bearing mice were treated with cisplatin (5 mg/kg) on the day of randomization. All five mice bearing the LU64 SCLC PDX had complete responses to SC16LD6.5 (1 mg/kg), with no recurring tumors up to 144 days of observation (Fig. 4A). Although LU64 also had a strong initial response to C/E, tumors recurred within 18 days (Fig. 4D). The LU86 PDX, which is refractory to C/E (Fig. 4E) (14), had complete and durable responses to SC16LD6.5 in a subset of tumor-bearing mice with a delta time to tumor progression (dTTP) versus IgG1LD6.5 of 32 days (Fig. 4B). SC16LD6.5 treatment of LU37 LCNEC PDX showed durable responses with a dTTP of 132 days (Fig. 4C), contrasting with cisplatin treatment that conferred a dTTP of only 4 days (Fig. 4F). An overview of all in vivo efficacy experiments with these and seven additional SCLC and LCNEC PDX tumor lines with varying levels of DLL3 expression is shown in Table 1.

In a further demonstration that in vivo efficacy was a result of DLL3 target–dependent toxin delivery, SCLC PDX tumors treated with either excess naked SC16 antibody dosed at as high as 30 mg/kg (30-fold excess of ADC dose) or the free drug, D6.5, dosed at 0.02 mg/kg Q4D×3 [equivalent to free drug load on SC16LD6.5 (1 mg/kg)] showed little to no inhibition of tumor growth relative to controls (fig. S7). Despite the fact that SC16LD6.5 is murine cross-reactive and mediates antigen-dependent cytotoxicity in cells expressing murine DLL3, treated mice continued to gain weight and showed no signs of lethargy. In contrast, mice treated with near maximum tolerated doses of SOC chemotherapeutic agents transiently lost weight and showed signs of lethargy common with such regimens (fig. S8). Collectively, SC16LD6.5 treatment of SCLC and LCNEC PDX resulted in effective and durable responses that significantly correlate with DLL3 expression (Pearson $r^2 = 0.58$, $P = 0.006$; Table 1 and Fig. 4G), often with greatly improved response over SOC chemotherapeutic regimens (Table 1).

We next explored the response to SC16LD6.5 in recurrent PDX tumors. LU64 tumors were first treated with SOC, to which they initially responded. Once these tumors recurred 35 days later, mice were re-randomized into four groups and treated with SC16LD6.5, IgG1LD6.5, vehicle, or a second round of C/E. All five recurring LU64 tumor–bearing mice treated with SC16LD6.5 showed a complete response after rebounding from first-line C/E treatment, whereas IgG1LD6.5 had no impact on tumor growth (Fig. 4H). A second round of C/E imparted a more transient response as compared to the initial response to C/E and was followed by rapid recurrence (Fig. 4I). Cumulatively, the above data demonstrate that SC16LD6.5 is efficacious in relapsed and refractory SCLC PDX tumors in vivo.

Many complete and durable responses were achieved in vivo with SC16LD6.5. To determine whether SC16LD6.5 prevents recurrence by targeting TICs, we treated mice bearing SCLC PDX with C/E or a single dose (1 mg/kg) of IgG1LD6.5 or SC16LD6.5. Five days after treatment, several mice with mean tumor volumes near the average of each cohort were euthanized, their tumors were harvested, and live human tumor cells were isolated by FACS. Limiting dilutions of isolated cells were retransplanted into at least four cohorts of mice from each original treatment group (table S4). This serial transplantation of cells in limiting dilutions from naïve or C/E-, IgG1LD6.5-, or SC16LD6.5-treated mice allowed for the estimation of residual TIC frequency using Poisson distribution statistics (Fig. 5, A and B). In these experiments, LU64 PDX tumors were shown to have a TIC frequency of 1:189 cells, which was reduced to 1:1136 cells in just 5 days after a single dose of SC16LD6.5 (Fig. 5C). In contrast, IgG1LD6.5 slightly increased, and C/E had no significant impact on the frequency of TICs in LU64 (1:78 and 1:248 cells, respectively; Fig. 5C). Similar robust impacts on the frequency of TICs were demonstrated with SC16LD6.5 in the LU95 SCLC PDX tumor (fig. S9, A and B), in which TICs are more frequent than in LU64 (1:60; Table 1). Notably, SC16LD6.5 administration to mice bearing the LU80 PDX, which have low DLL3 expression, did not alter TIC frequency (fig. S9, C and D). These data provide functional evidence that the tumor growth inhibition and durable responses observed in vivo in response to SC16LD6.5 result from the effective targeting and eradication of DLL3-expressing TICs.

Exploratory toxicology

The preclinical safety profile of SC16LD6.5 was further characterized in repeat-dose studies both in rats (once every 2 weeks for 2 cycles, followed by a 6-week recovery period for a subset of the animals) and in cyno (once every 3 weeks for 3 cycles, followed by a 6-week recovery period for a subset of the animals). Both species are relevant toxicology models, given the antibody cross-reactivity to rat and cyno DLL3 (table S3). Observed toxicities consisted of reversible trilineage myelosuppression, mild kidney degeneration, and skin thickening and hyperpigmentation (fig. S10), each of which is attributable to off-target toxicity associated with the PBD linker drug and has been observed with PBDs (46). Together, the above safety profile and efficacy data supported the initiation of a phase 1 clinical trial (NCT01901653) in recurrent or refractory high-grade pulmonary neuroendocrine cancer patients.

DISCUSSION

Here, we show that SC16LD6.5, a DLL3-targeted ADC, induces durable responses in SCLC and LCNEC PDX tumor models after a single course of therapy. Administration of high doses of naked anti-DLL3 antibody or the ADC dose equivalent of the free PBD dimer toxin showed little to no impact on tumor growth, supporting the hypothesis that SC16LD6.5 efficacy is mediated by targeted delivery of the toxin to DLL3-expressing tumor cells. The observed durable responses after SC16LD6.5 exposure are consistent with the effective targeting of TICs, in contrast with the SOC C/E, which neither affected the frequency of TICs nor provided durable responses. We hypothesize that the frequent and rapid relapse

observed clinically among SCLC patients despite strong initial debulking responses to C/E is consistent with the inability of SOC to affect TIC frequency (4).

One preconception that accompanies the cancer stem cell paradigm is that these cells are rare (12). We show that TICs in SCLC are relatively frequent (~1:177 cells; range, 1:31 to 1:388), and we have evidence to suggest a higher frequency of TICs in LCNEC PDX. By IHC and flow cytometry, DLL3 expression is seen throughout the tumor, with most cells expressing the antigen at some level. The rapid tumor debulking seen with SC16LD6.5 is likely mediated by DLL3 expression on most tumor cells, whereas the sustained progression-free responses are due to DLL3 expression on TICs. The sustained responses observed in the single-agent efficacy studies executed here offer the promise of more durable responses in the clinic. Furthermore, they suggest that patients in the clinic may not need to be dosed until progression, but rather a limited number of treatment cycles may be adequate to drive improvements in survival endpoints—a true test of the cancer stem cell hypothesis.

Targeted cancer therapies that inhibit driver oncogene mutations have the advantage of being highly tumor-specific, which generally translates to a substantial safety window. However, because these tumors are addicted to the oncogene, drug resistance frequently emerges through compensatory mutations or reactivation of the signaling pathway by way of mutations in other genes (47). SCLC and LCNEC tumors have elevated expression of the neuroendocrine transcription factor *ASCL1*, which is a lineage oncogene critical to neuroendocrine tumorigenesis (24, 37, 48, 49). *DLL3* appears to be transcriptionally regulated by ASCL1 (36, 37), and a strong correlation of expression is indeed observed for these genes in SCLC and LCNEC PDX tumor models. The lone exception is LU86, which has DLL3 expression despite minimal *ASCL1* expression. The role of *DLL3* in the process of SCLC tumorigenesis is unknown. Whether *DLL3* is an ASCL1-induced driver of neuroendocrine tumors or simply a passenger in tumors that are addicted to ASCL1 has implications for potential emergence of resistance to SC16LD6.5. If DLL3 is elevated as a consequence of ASCL1 overexpression, it serves as an excellent surface protein for the $ASCL1^{+}$ phenotype and can act as a Trojan horse for toxin delivery. Moreover, if DLL3 is in fact a driver of tumorigenesis, its down-regulation to evade SC16LD6.5 should result in slowed tumor growth due to Notch reactivation.

ADC targets must have an extracellular epitope amenable to specific antibody binding and be capable of internalization. Upon initial consideration, DLL3 may not appear to be a good ADC target because murine DLL3 was reported to localize to the Golgi and cytoplasmic vesicles in the presomitic mesoderm (27, 28, 35). In contrast, our results demonstrate by IHC and flow cytometry that human DLL3 is detectable on the surface of high-grade pulmonary neuroendocrine tumor cells. Furthermore, IHC analyses on primary tumors from various sources revealed DLL3 membrane expression in ~89% of SCLC tumors and 84% of LCNEC tumors. DLL3 expression in PDX tumors further correlated with response to SC16LD6.5, and it is apparent that even modest expression of DLL3 permits ADC-mediated cytotoxicity in vitro and in vivo. This activity likely reflects the rapid internalization of DLL3 in tumor cells.

In addition to the specific antibody used in an ADC, the choice of toxin payload influences efficacy, toxicity, and the likelihood of development of resistance. PBD dimers are a class of payloads that bind in the minor groove of DNA, where they form covalent aminal cross-links between the N2 of guanine and the C11 position of the PBD. The resulting PBD-DNA adducts cause replication forks to stall and tumor cells to arrest at the G_2-M boundary, ultimately resulting in apoptosis at low nanomolar to picomolar concentrations (50, 51). PBD dimers are particularly potent because of their cell cycle–independent activity and because their integration minimally distorts DNA, increasing the likelihood of evasion of DNA damage repair responses (51). Because of the potency of PBD dimers and similar cell cycle–independent payloads, normal tissues accessed by such potently armed ADCs must be devoid of target expression. DLL3 meets this criterion.

The availability of a large high-grade pulmonary neuroendocrine PDX tumor repository facilitated the discovery and validation of DLL3 as a therapeutic target. One limitation of the PDX tumor models studied here is that all were initiated from treatment-naïve SCLC or LCNEC patients. Patients encountered in early clinical studies will have received at least first-line SOC chemotherapy and have recurrent or refractory disease. We show here that treatment of SCLC PDX tumors with SOC chemotherapy followed by second-line therapy with SC16LD6.5 upon recurrence was as effective as first-line therapy with SC16LD6.5. Additionally, efficacy in the chemorefractory LU86 PDX tumor model suggests that patients with tumors resistant to SOC will still respond to SC16LD6.5. Furthermore, IHC showed high DLL3 protein expression in 85% of recurrent and refractory SCLC tumors, supporting the hypothesis that SC16LD6.5 should be effective in patients encountered in the setting of second- and third-line treatments.

High-grade pulmonary neuroendocrine tumors metastasize throughout the lungs, lymph nodes, adrenal gland, bone, brain, and liver (2). Although PDX tumors grown subcutaneously are arguably a model of metastasis because they represent tumors growing in a nonorthotopic site, a limitation of PDX models is their lack of systemic metastases. IHC data suggest equivalent expression of DLL3 in both primary and meta-static sites in patients, implying that SC16LD6.5 will effectively address ADC-accessible metastases. It is not expected that SC16LD6.5 will cross the blood-brain barrier; however, brain metastases can be addressed with cranial irradiation. It is also unclear whether SC16LD6.5 will be able to efficiently penetrate large tumors in patients compared to those encountered here in PDX models.

Several lines of evidence support the hypotheses that ASCL1 drives high-grade pulmonary neuroendocrine tumorigenesis (21, 24) and induces expression of Notch ligands (36, 37, 52), and that Notch pathway inhibition promotes neuroendocrine cell fate decisions (25, 34). Elevated expression of DLL3, a protein that interferes with Notch signaling (27, 35), in high-grade pulmonary neuroendocrine tumors may unify these observations. Regardless, by targeting a cytotoxic payload to DLL3-expressing TICs with a monoclonal antibody, SC16LD6.5 offers a therapeutic approach to the treatment of high-grade pulmonary neuroendocrine tumors by delivering a potent cytotoxin specifically to tumor cells and avoiding normal tissues. The increased DLL3 expression in tumors compared to normal

tissues and the observed tolerability in preclinical rat and cynomolgus models suggest that a clinically relevant dose can be safely achieved in patients.

MATERIALS AND METHODS

Study design

The objective of in vivo efficacy studies was to evaluate the activity of SC16LD6.5 in PDX tumor models. Sample size (n = 5 to 8 mice per group) was determined on the basis of consistency and homogeneity of PDX tumor growth in the various models and was sufficient to determine statistically significant differences in tumor response between the various treatment groups. Animals were randomized on the basis of tumor size so that each treatment group had average tumor volumes of 140 to 200 mm^3. Tumors were measured with digital calipers in two dimensions, long and short axis (in millimeters), and tumor volume (mm^3) was calculated as the volume of a prolate ellipsoid: 0.5 × long axis × short $axis^2$. Tumor measurements for individual mice were plotted. Data collection was stopped, and the mice were euthanized if they exhibited ≥20% weight loss, inactivity, or poor body condition; when individual tumors reached ≥1000 mm^3; when the average tumor volume of a given treatment group reached ≥800 mm^3; or when the study reached 150 days after randomization. Ten NOD/SCID mice in the SOC group that were euthanized because of chemo-related toxicities within 21 days after treatment were excluded from the reported data. Four individual mice (two treated with IgG1LD6.5 and two treated with SC16LD6.5) that were euthanized because of non–cancer-related illness within 40 days after treatment were excluded from the TTP calculations. No additional outliers were excluded from the data.

PDX tumor model propagation

SCLC and LCNEC PDX tumor models were initiated as previously described (14) and propagated in 5- to 7-week-old female NOD/SCID mice (Harlan Laboratories and Charles River Laboratories) by subcutaneous implantation of dissociated cells into a single site near the lower mammary fat pad. Animal health was monitored daily, and mouse weights and tumor volumes were measured at least weekly. All in vivo protocols were approved by the Stemcentrx Institutional Animal Care and Use Committee (protocols SCAR-3-2008 and SCAR-5-2008) and performed in accordance with the American Association for Laboratory Animal Science and American Veterinary Medical Association guidelines. All experiments described herein were performed using PDXs from passages 1 to 4.

RNA isolation and mRNA expression analysis

RNA was isolated with the RNeasy Mini Kit (Qiagen) following the manufacturer’s instructions and stored at −80°C. For whole transcriptome analysis, complementary DNA (cDNA) was generated from 1 ng of RNA using the Ovation RNA-Seq System V2 (NuGEN Technologies). The resulting cDNA library was fragmented, and barcode adapters were added to allow pooling of fragment libraries from different samples. Whole transcriptome sequencing was performed using the Sequencing by Oligo Ligation/Detection (SOLiD) 4.5 or SOLiD 5500×l system (Life Technologies). Data were mapped to 34,609 genes as annotated by RefSeq version 47 using NCBI (National Center for Biotechnology

Information) version hg19.2 of the published human genome, and data for *DLL3* are available (table S5).

For qRT-PCR, cDNA was generated from 1 ng of RNA, using the High-Capacity cDNA Reverse Transcription Kit (Life Technologies) following the manufacturer's instructions. Each cDNA sample was preamplified with 0.2× TaqMan assay specific to *DLL3, ASCL1, NEUROD1, ACTB*, and *ALAS1* (Life Technologies) diluted in DNA suspension buffer (Teknova), using the 1× TaqMan PreAmp Master Mix (Life Technologies) according to the manufacturer's instructions. The preamplified cDNA was combined with 1× TaqMan Gene Expression Master Mix (Life Technologies) and 1× GE Sample Loading Reagent (Fluidigm), 1× of each individual TaqMan assays was mixed with 1× Assay Loading Reagent (Fluidigm), and reaction mixes were run on the Fluidigm BioMark according to the manufacturer's instructions. Fluidigm Data Collection Software was used to set the threshold for each TaqMan assay, data were normalized to the average of the endogenous controls (*ACTB* and *ALAS*), and expression was calculated for each sample relative to the average expression in normal tissues (relative expression, $2^{-\Delta\Delta Ct}$). Technical triplicates were run for qRT-PCR on two to three biological replicates for each sample, and relative expression values were averaged.

RNA(1 μg) from PDX lines was analyzed with the Agilent SurePrint GE Human 8×60 v2 microarray platform and the R statistical environment (v2.14.2). Microarray data are the average of two biological replicates for each PDX. Standard industry practices were used to quantile-normalize the background-subtracted intensity values, using the preprocessCore Bioconductor R package (53).

Subcloning of *DLL3* expression and lentiviral constructs and cell line engineering

The human DLL3 extracellular domain (ECD) His fusion protein was made by PCR amplification from a commercially available cDNA (SC111951, Origene) followed by subcloning into pEE12.4 expression plasmid (Lonza) modified to encode an IgK signal peptide upstream of *DLL3*, with a C-terminal 6×His epitope tag (pEE12.4-h*DLL3*). Constructs encoding soluble cyno (pEE12.4-c*DLL3*) and rat *DLL3* (pEE12.4-r*Dll3*) ECD were similarly constructed using synthetic codonoptimized c*DLL3* and r*Dll3* open reading frames (ORFs; GeneWiz) as templates for PCR amplification. The encoded DLL3 ECD identity between various species is as follows: human-cynomolgus, 96%; human-rat, 82%; human-mouse, 83%; rat-mouse, 94%. HEK-293T cells expressing human *DLL3* (HEK-293T.h*DLL3*) were made by transduction of HEK-293T cells (American Type Culture Collection) using a lentivirus made from a commercial bicistronic lentiviral vector (Open Biosystems) that expresses both human DLL3 and green fluorescent protein (GFP) under the control of a constitutive cytomegalovirus promoter. HEK-293T cells expressing full-length cynomolgus *DLL3* (HEK-293T.c*DLL3*) or rat *Dll3* (HEK-293T.r*Dll3*) were made by subcloning the respective ORF into a lentiviral expression plasmid (pCDH-EF1-MCS-T2A-GFP, System Biosciences). Transduced cells were single-cell sorted with FACSAria (BD Biosciences), and individual clones were screened by flow cytometry for stable expression of DLL3 and GFP. HEK-293T.h*DLL3* and parental HEK-293T were cultured in Dulbecco's modified Eagle's medium (DMEM; Corning) containing 10% fetal

bovine serum (FBS; Hyclone) in tissue culture flasks (BD Falcon) at 37°C in a humidified incubator with 5% CO_2. Cells were passaged every 2 to 4 days. Quantitation of viral particles was done with the p24 ELISA kit (Cell Biolabs).

Enzyme-linked immunosorbent assay

Recombinant His-tagged DLL1 and DLL4 (R&D Systems) or DLL3 produced from pEE12.4-h*DLL3* as a His fusion protein in CHO cells were immobilized on high protein binding 96-well ELISA plates (Greiner Microlon) at 1 μg/ml in phosphate-buffered saline (PBS) overnight at 4°C. Plates were blocked with PBS plus 3% bovine serum albumin (BSA) and washed in PBS with 0.05%Tween 20 (PBST). Serial dilutions of SC16 or a human IgG1 isotype control in PBST containing 1% BSA (PBSTA) were added to the plate and incubated for 2 hours at room temperature (RT). After washing with PBST, a 1:2000 dilution of a donkey anti-human IgG horseradish peroxidase (HRP) conjugate (Jackson ImmunoResearch) in PBSTA was added to the plates for 1 hour. SC16 binding was visualized using Ultra-TMB substrate (Thermo Fisher Scientific), and plates were read at 450-nm absorbance.

Protein expression in tissue and tumor lysates

PDX tumors were excised from mice and flash-frozen on dry ice/ethanol, and flash-frozen pieces of normal human tissues were purchased (Asterand). Protein extraction buffer (Biochain Institute) was added to thawed samples, and the samples were pulverized using the TissueLyser kit (Qiagen) according to the manufacturer's instructions. Lysates were cleared by centrifugation (20,000*g* for 20 min, 4°C) and stored at −80°C. Total protein was quantified using bicinchoninic acid. Standard 384-well plates [Meso Scale Discovery (MSD)] were coated overnight at 4°C with 15 μl of an anti-DLL3 antibody at 4 μg/ml in PBS. The next day, the plates were washed in PBST and blocked in 35 μl of PBS plus 3% BSA for 1 hour. The plates were washed again in PBST. Ten microliters of 10× diluted lysate in PBSTA or serially diluted recombinant DLL3 standard in PBSTA containing 10% protein extraction buffer was also added to the wells and incubated at RT for 2 hours. The plates were washed in PBST, and 10 μl of a second anti-DLL3 antibody recognizing a different epitope conjugated to MSD SULFO-TAG (MSD) was added to the washed plates at 0.5 μg/ml in PBSTA. The plates were washed in PBST, and 35 μl of 1× Read Buffer T with surfactant (MSD) was added to each well. The plates were read on a SECTOR Imager 2400. Raw signals were interpolated to a DLL3 standard curve using a Workbench analysis program to derive DLL3 concentrations in test samples. Values were then divided by total protein concentration to yield a readout of ppm (ng DLL3 protein/mg total protein).

Immunohistochemistry

IHC was performed on 5-μm-thick formalin-fixed, paraffin-embedded tissue sections mounted on glass slides. The slides were deparaffinized in xylene and rehydrated through graded alcohols to water. The slides were pretreated with Target Retrieval Solution (Dako) for 20 min at 99°C and treated with 0.3% hydrogen peroxide in tris-buffered saline for 8 min, followed by incubation with an avidin/biotin blocking kit (Vector Laboratories). Nonspecific IgG binding was blocked with 10% horse serum in 3% BSA in PBS. Anti-DLL3 antibody or murine IgG2a isotype control at 10 μg/ml was added on the slides,

followed by incubation for 60 min at RT. The competition assay used 5 M excess of DLL3-His protein preincubated with the DLL3 antibody before incubating on tissue sections. The slides were rinsed and then incubated with biotin-conjugated horse anti-mouse secondary antibody (Vector Laboratories) for 30 min at RT. The slides were incubated with Vectastain ABC Elite (Vector Laboratories) reagents for 30 min at RT, and primary tumor samples, but not PDX, were incubated in tyramide signal amplification (PerkinElmer) diluted in amplification buffer at 1:25 and incubated on the slides for 5 min at RT. After washes, the slides were incubated in streptavidin-HRP (PerkinElmer) diluted at 1:100 for 30 min at RT and then incubated in Metal Enhanced DAB (Thermo Fisher Scientific). The slides were then counterstained, dehydrated, and coverslipped. A person with more than 15 years of IHC experience scored the samples, and *H*-scores were calculated using membranous staining intensity and percentage of positive cells. The researcher scoring the samples was blinded to the corresponding pathology report and diagnosis of each sample but is knowledgeable in lung cancer pathology and can distinguish SCLC, NSCLC, and normal lung pathology.

Flow cytometry

PDX tumors were disaggregated to single-cell suspensions by mincing with razor blades and passing through 40-μm nylon filters. The cells were incubated with fluorophore-conjugated antibodies for 20 min, washed three times, suspended in 4′,6′-diamidino-2-phenylindole (DAPI; 2 μg/ml), then analyzed on a BD FACSAria I. The antibodies used were fluorescein isothiocyanate (FITC) anti-mouse CD45 (clone 30-F11, BioLegend), FITC anti-human CD45 (clone HI30, BioLegend), FITC anti-mouse H-2Kd (clone SF1-1.1,BioLegend), peridinin chlorophyll protein (PerCP)–Cy5.5 anti-human EpCAM (clone 9C4, BioLegend), and PE or Alexa Fluor 647 (AF647) anti-human DLL3.The cells were suspended in DAPI (2 μg/ml) for analysis on a FACSCanto II (BD Biosciences).

HEK-293T.h*DLL3*, HEK-293T.c*DLL3*, and HEK-293T.r*Dll3* were harvested with Versene (Life Technologies), washed with PBS, and resuspended in Hepes with 2% FBS (assay buffer) at 2.5×10^6 cells/ml. A portion (40 μl) of this cell suspension was added per well to a 96-well plate followed by the addition of twofold serial dilutions of SC16LD6.5 in assay buffer. Each SC16LD6.5 concentration was tested in duplicate. Cells were mixed well and incubated at 2° to 8°C for 2 hours with intermittent agitation of the plate. At the end of the incubation, the cells were washed twice with assay buffer followed by incubation with antihuman IgG antibody (4 μg/ml) conjugated to AF647. After 45 min at 2° to 8°C in the dark, the cells were washed twice with PBS followed by a 10-min incubation with Fixable Viability Dye eFluor 450 (E Bioscience), which can irreversibly stain dead cells before fixation. Paraformaldehyde (1%) in PBS was then added to fix the cells before analysis with a BD FACSCanto II flow cytometer. Viable cells were selected and analyzed for AF647 fluorescence intensity. Rainbow beads (BD Biosciences) were used as calibrators to transform mean fluorescence intensities into MESF in the Cy5 channel. MESF values were plotted as a function of SC16LD6.5 concentration. Data were analyzed with Prism software using a four-parameter logistic nonlinear regression model to calculate the Bmax (maximum binding) values for each cell line as a reflection of the relative DLL3 expression of each cell line. Each Bmax value was set to 100% to normalize for expression level and plotted against SC16LD6.5 concentration.

In vitro killing

The cytotoxicity of various antibodies was tested on HEK-293T, HEK-293T.h*DLL3*, LU64, and LU37. HEK-293T cells were plated in culture medium (DMEM + 10% FBS) (50 μl per well) at 500 cells per well in 96-well tissue culture–treated plates on day 1. LU64 and LU37 tumors were removed from mice, dissociated to single-cell suspensions, and plated under serum-free conditions at 2500 cells per well on Primaria plates (BD Falcon) at 50 μl per well in DMEM/F12 (Mediatech). The HEK-293T plates were incubated overnight in a humidified incubator at 37°C containing 5% CO_2, and patient-derived samples were incubated with 5% CO_2 and 5% O_2. On day 2, D6.5, SC16, SC16LD6.5, or IgG1LD6.5 serial dilutions (50 μl per well) were added to the plates, and cells were allowed to proliferate for 4 days (HEK-293T cells) and 7 days (patient-derived samples). Each sample concentration was tested in triplicate. Cell viability was measured with the CellTiter-Glo (Promega Corporation) reagent according to the manufacturer's instructions, using the Victor plate reader (PerkinElmer Corporation). The luminescence values for each sample-treated well were normalized to the values obtained for untreated wells, and percent cell viability was plotted as a function of sample concentration. Data were analyzed with GraphPad Prism software using a four-parameter logistic nonlinear regression model.

Lentiviral shRNA mediated expression knockdown

Lentiviral particles containing *DLL3* shRNA were generated according to standard lentiviral production procedures (GE Dharmacon). Quantitation of viral particles was done with the p24 ELISA kit (Cell Biolabs). Dissociated cells from LU37 PDX line were transduced with lentiviral particles at a multiplicity of infection of 3 and incubated for 72 hours on Primaria plates (Corning) in a humidified incubator at 37°C containing 5% O_2 and 5% CO_2.

Internalization

HEK-293T.h*DLL3* or HEK-293T cells were seeded (250,000 cells per well) in tissue culture–treated six-well plates (Greiner BioOne) in 2 ml of culture medium and 100 μl of the BacMam reagent (Life Technologies) for 48 hours. BacMam is a modified baculovirus that infects mammalian cells and encodes for the constitutive expression of a fusion protein consisting of SLP-1 fused to RFP. Previous reports have demonstrated that SLP-1 is a marker of late endosomal intracellular compartments (43). Cells were harvested, washed, and stained in FSM buffer containing SC16, SC16LD6.5, or control reagents (5 μg/ml) for 30 min at 4°C. After washing, a secondary anti-human IgG AF647 conjugate (Life Technologies), diluted 1:200 in FSM buffer, was added for another 30 min at 4°C. The samples were washed in culture medium at 4°C, resuspended in cold culture medium containing 500 nM Calcein AM (Life Technologies), and seeded into two 96-well flat-bottomed tissue culture plates. One plate was strictly kept at 4°C for 3 hours, whereas the second plate was incubated at 37°C in an incubator with 5% CO_2. After incubation, the plates were imaged with fluorescein (Calcein), rhodamine (RFP), and Cy5 (AF647) filters within a 10-min period, using an ImageXpressMicro imager (Molecular Devices). Images were separately analyzed for each fluorescent color, and composite images with false color were assembled in a second step to visualize fluorescent colocalization (MetaXpress 4.0). The MetaXpress software was also used to identify and count all viable cells (Calcein-

positive) with colocalization events for SLP-1 (RFP; false color displayed as green) and human IgG (AF647).

In vivo efficacy in xenografts

Female NOD/SCID mice (Harlan Laboratories; Charles River Laboratories) were implanted with 50,000 PDX tumor cells and randomized into groups of five to eight animals with average tumor volumes of 140 to 200 mm^3 per cohort, typically 5 to 8 weeks after implantation. Mice were treated with vehicle (5% glucose/saline or saline, intraperitoneally, day 1), cisplatin (5 mg/kg, intraperitoneally, day 1; Besse Medical), etoposide (8 mg/kg, intraperitoneally, days 1, 2, and 3; Besse Medical), control IgG1LD6.5 [0.3 to 1 mg/kg, intraperitoneally, days 1, 5, and 9 (Q4D×3)], or SC16.LD6.5 [0.3 to 1 mg/kg, intraperitoneally, days 1, 5, and 9 (Q4D×3)]. Efficacy was measured by calculating the %TGI and TTP. %TGI was calculated as the tumor volume change between the arithmetic mean tumor volumes in the vehicle-treated control group on the day the first control-treated mouse was euthanized because tumor volume reached≥1000 mm^3 and the arithmetic mean tumor volume in the test cohort on that day. A TTP for each individual mouse was recorded as the number of days between treatment day and the day when tumor burden reached 50 mm3 above nadir, or the study length in days after treatment if a durable response was observed, and then the median TTP value was determined for each treatment group. A dTTP was calculated by subtracting the TTP for a control group (vehicle or IgG1LD6.5, respectively) from the TTP of a treatment group (SOC or SC16.LD6.5, respectively).

Limiting dilution assay

After euthanasia of representative mice from each treatment group assessed, live human cells were sorted on a FACSAria I (BD Biosciences), and cohorts of 8 to 10 mice were injected with decreasing numbers of live human cells, ranging from 2500 down to 3 cells. Tumor-negative mice dying before 16 weeks after implant were excluded from the analysis. Mice were scored positive for tumor growth once their tumor size exceeded 200 mm^3. Estimates of TIC frequency were calculated using the L-Calc software package (Stem Cell Technologies) to apply Poisson distribution analysis to the frequencies of tumor-negative mice at each injected cell number.

Statistical analysis

Tumor growth curves are shown for individual animals in all representative in vivo experiments. The number of biological and technical replicates and the statistical tests run for various experiments are detailed in the corresponding Materials and Methods or Results section. A Pearson correlation was assessed in GraphPad Prism. P values reflect two-tailed unpaired t test analyses, with an F test confirming significant variance. Bars shown on vertical scatter plots represent the geometric mean or mean for each group, as detailed in the figure legends. P values ≤0.05 were considered statistically significant.

Supplementary Material

Refer to Web version on PubMed Central for supplementary material.

Acknowledgments

We would like to acknowledge the contributions of the members of Stemcentrx In Vivo Biology Team and of A. Conner, S. Lazetic, C. Lee, E. Bishop, M. Richardson, and P. Lindley.

Funding: This study was funded by Stemcentrx Inc., a privately held and financed company. J.J. is supported by the Central and East European Oncology Group. M.C.P. is supported, in part, by the National Cancer Institute of the NIH under award number P30 CA008748 (recipient is C. Thompson).

REFERENCES AND NOTES

1. Rekhtman N. Neuroendocrine tumors of the lung: An update. Arch. Pathol. Lab. Med. 2010; 134:1628–1638. [PubMed: 21043816]
2. Travis WD. Pathology and diagnosis of neuroendocrine tumors: Lung neuroendocrine. Thorac. Surg. Clin. 2014; 24:257–266. [PubMed: 25065926]
3. William WN Jr, Glisson BS. Novel strategies for the treatment of small-cell lung carcinoma. Nat. Rev. Clin. Oncol. 2011; 8:611–619. [PubMed: 21691321]
4. Joshi M, Ayoola A, Belani CP. Small-cell lung cancer: An update on targeted therapies. Adv. Exp. Med. Biol. 2013; 779:385–404. [PubMed: 23288650]
5. Eichhorn F, Dienemann H, Muley T, Warth A, Hoffmann H. Predictors of survival after operation among patients with large cell neuroendocrine carcinoma of the lung. Ann. Thorac. Surg. 2015; 99:983–989. [PubMed: 25596870]
6. Merrill RM, Henson DE, Barnes M. Conditional survival among patients with carcinoma of the lung. Chest. 1999; 116:697–703. [PubMed: 10492274]
7. von Pawel J, Jotte R, Spigel DR, O'Brien ME, Socinski MA, Mezger J, Steins M, Bosquée L, Bubis J, Nackaerts K, Trigo JM, Clingan P, Schütte W, Lorigan P, Reck M, Domine M, Shepherd FA, Li S, Renschler MF. Randomized phase III trial of amrubicin versus topotecan as second-line treatment for patients with small-cell lung cancer. J Clin. Oncol. 2014; 32:4012–4019. [PubMed: 25385727]
8. van de Stolpe A. On the origin and destination of cancer stem cells: A conceptual evaluation. Am. J. Cancer Res. 2013; 3:107–116. [PubMed: 23359140]
9. Travis WD. Advances in neuroendocrine lung tumors. Ann. Oncol. 2010; 21:vii65–vii71. [PubMed: 20943645]
10. Clinical Lung Cancer Genome Project (CLCGP), Network Genomic Medicine (NGM). A genomics-based classification of human lung tumors. Sci. Transl. Med. 2013; 5:209ra153.
11. Rudin CM, Durinck S, Stawiski EW, Poirier JT, Modrusan Z, Shames DS, Bergbower EA, Guan Y, Shin J, Guillory J, Rivers CS, Foo CK, Bhatt D, Stinson J, Gnad F, Haverty PM, Gentleman R, Chaudhuri S, Janakiraman V, Jaiswal BS, Parikh C, Yuan W, Zhang Z, Koeppen H, Wu TD, Stern HM, Yauch RL, Huffman KE, Paskulin DD, Illei PB, Varella-Garcia M, Gazdar AF, de Sauvage FJ, Bourgon R, Minna JD, Brock MV, Seshagiri S. Comprehensive genomic analysis identifies *SOX2* as a frequently amplified gene in small-cell lung cancer. Nat. Genet. 2012; 44:1111–1116. [PubMed: 22941189]
12. Williams SA, Anderson WC, Santaguida MT, Dylla SJ. Patient-derived xenografts, the cancer stem cell paradigm, and cancer pathobiology in the 21st century. Lab. Invest. 2013; 93:970–982. [PubMed: 23917877]
13. Rosfjord E, Lucas J, Li G, Gerber H-P. Advances in patient-derived tumor xenografts: From target identification to predicting clinical response rates in oncology. Biochem. Pharmacol. 2014; 91:135–143. [PubMed: 24950467]
14. Anderson WC, Boyd MB, Aguilar J, Pickell B, Laysang A, Pysz MA, Bheddah S, Ramoth J, Slingerland BC, Dylla SJ, Rubio ER. Initiation and characterization of small cell lung cancer patient-derived xenografts from ultrasound-guided transbronchial needle aspirates. PLOS One. 2015; 10:e0125255. [PubMed: 25955027]
15. Poirier JT, Gardner EE, Connis N, Moreira AL, de Stanchina E, Hann CL, Rudin CM. DNA methylation in small cell lung cancer defines distinct disease subtypes and correlates with high expression of EZH2. Oncogene. 2015

16. Reynolds SD, Giangreco A, Power JHT, Stripp BR. Neuroepithelial bodies of pulmonary airways serve as a reservoir of progenitor cells capable of epithelial regeneration. Am. J. Pathol. 2000; 156:269–278. [PubMed: 10623675]

17. Park K-S, Liang M-C, Raiser DM, Zamponi R, Roach RR, Curtis SJ, Walton Z, Schaffer BE, Roake CM, Zmoos A-F, Kriegel C, Wong K-K, Sage J, Kim CF. Characterization of the cell of origin for small cell lung cancer. Cell Cycle. 2011; 10:2806–2815. [PubMed: 21822053]

18. Song H, Yao E, Lin C, Gacayan R, Chen M-H, Chuang P-T. Functional characterization of pulmonary neuroendocrine cells in lung development, injury, and tumorigenesis. Proc. Natl. Acad. Sci. U.S.A. 2012; 109:17531–17536. [PubMed: 23047698]

19. Sutherland KD, Proost N, Brouns I, Adriaensen D, Song J-Y, Berns A. Cell of origin of small cell lung cancer: Inactivation of *Trp53* and *Rb1* in distinct cell types of adult mouse lung. Cancer Cell. 2011; 19:754–764. [PubMed: 21665149]

20. Ball DW. Achaete–scute homolog-1 and Notch in lung neuroendocrine development and cancer. Cancer Lett. 2004; 204:159–169. [PubMed: 15013215]

21. Borges M, Linnoila RI, van de Velde HJK, Chen H, Nelkin BD, Mabry M, Baylin SB, Ball DW. An *achaete-scute* homologue essential for neuroendocrine differentiation in the lung. Nature. 1997; 386:852–855. [PubMed: 9126746]

22. Guillemot F, Lo L-C, Johnson JE, Auerbach A, Anderson DJ, Joyner AL. Mammalian *achaete-scute* homolog 1 is required for the early development of olfactory and autonomic neurons. Cell. 1993; 75:463–476. [PubMed: 8221886]

23. Li Y, Linnoila RI. Multidirectional differentiation of Achaete–Scute homologue–1–defined progenitors in lung development and injury repair. Am. J. Respir. Cell Mol. Biol. 2012; 47:768–775. [PubMed: 22878413]

24. Jiang T, Collins BJ, Jin N, Watkins DN, Brock MV, Matsui W, Nelkin BD, Ball DW. Achaete-scute complex homologue 1 regulates tumor-initiating capacity in human small cell lung cancer. Cancer Res. 2009; 69:845–854. [PubMed: 19176379]

25. Morimoto M, Nishinakamura R, Saga Y, Kopan R. Different assemblies of Notch receptors coordinate the distribution of the major bronchial Clara, ciliated and neuroendocrine cells. Development. 2012; 139:4365–4373. [PubMed: 23132245]

26. Ntziachristos P, Lim JS, Sage J, Aifantis I. From fly wings to targeted cancer therapies: A centennial for notch signaling. Cancer Cell. 2014; 25:318–334. [PubMed: 24651013]

27. Chapman G, Sparrow DB, Kremmer E, Dunwoodie SL. Notch inhibition by the ligand Delta-Like 3 defines the mechanism of abnormal vertebral segmentation in spondylocostal dysostosis. Hum. Mol. Genet. 2011; 20:905–916. [PubMed: 21147753]

28. Geffers I, Serth K, Chapman G, Jaekel R, Schuster-Gossler K, Cordes R, Sparrow DB, Kremmer E, Dunwoodie SL, Klein T, Gossler A. Divergent functions and distinct localization of the Notch ligands DLL1 and DLL3 in vivo. J Cell Biol. 2007; 178:465–476. [PubMed: 17664336]

29. Fehon RG, Kooh PJ, Rebay I, Regan CL, Xu T, Muskavitch MA, Artavanis-Tsakonas S. Molecular interactions between the protein products of the neurogenic loci *Notch* and *Delta*, two EGF-homologous genes in Drosophila. Cell. 1990; 61:523–534. [PubMed: 2185893]

30. Dunwoodie SL, Henrique D, Harrison SM, Beddington RS. Mouse *Dll3*: A novel divergent *Delta* gene which may complement the function of other *Delta* homologues during early pattern formation in the mouse embryo. Development. 1997; 124:3065–3076. [PubMed: 9272948]

31. Ladi E, Nichols JT, Ge W, Miyamoto A, Yao C, Yang L-T, Boulter J, Sun YE, Kintner C, Weinmaster G. The divergent DSL ligand Dll3 does not activate Notch signaling but cell autonomously attenuates signaling induced by other DSL ligands. J Cell Biol. 2005; 170:983–992. [PubMed: 16144902]

32. Loomes KM, Stevens SA, O'Brien ML, Gonzalez DM, Ryan MJ, Segalov M, Dormans NJ, Mimoto MS, Gibson JD, Sewell W, Schaffer AA, Nah H-D, Rappaport EF, Pratt SC, Dunwoodie SL, Kusumi K. *Dll3* and *Notch1* genetic interactions model axial segmental and craniofacial malformations of human birth defects. Dev. Dyn. 2007; 236:2943–2951. [PubMed: 17849441]

33. Espinoza I, Miele L. Notch inhibitors for cancer treatment. Pharmacol. Ther. 2013; 139:95–110. [PubMed: 23458608]

34. Kunnimalaiyaan M, Chen H. Tumor suppressor role of Notch-1 signaling in neuroendocrine tumors. Oncologist. 2007; 12:535–542. [PubMed: 17522241]
35. Serth K, Schuster-Gossler K, Kremmer E, Hansen B, Marohn-Köhn B, Gossler A. O-Fucosylation of DLL3 is required for its function during somitogenesis. PLOS One. 2015; 10:e0123776. [PubMed: 25856312]
36. Henke RM, Meredith DM, Borromeo MD, Savage TK, Johnson JE. Ascl1 and Neurog2 form novel complexes and regulate *Delta-like3 (Dll3)* expression in the neural tube. Dev. Biol. 2009; 328:529–540. [PubMed: 19389376]
37. Augustyn A, Borromeo M, Wang T, Fujimoto J, Shao C, Dospoy PD, Lee V, Tan C, Sullivan JP, Larsen JE, Girard L, Behrens C, Wistuba II, Xie Y, Cobb MH, Gazdar AF, Johnson JE, Minna JD. ASCL1 is a lineage oncogene providing therapeutic targets for high-grade neuroendocrine lung cancers. Proc. Natl. Acad. Sci. U.S.A. 2014; 111:14788–14793. [PubMed: 25267614]
38. Bouchard H, Viskov C, Garcia-Echeverria C. Antibody–drug conjugates—a new wave of cancer drugs. Bioorg. Med. Chem. Lett. 2014; 24:5357–5363. [PubMed: 25455482]
39. Pedersen N, Mortensen S, Sørensen SB, Pedersen MW, Rieneck K, Bovin LF, Poulsen HS. Transcriptional gene expression profiling of small cell lung cancer cells. Cancer Res. 2003; 63:1943–1953. [PubMed: 12702587]
40. Poirier JT, Dobromilskaya I, Moriarty WF, Peacock CD, Hann CL, Rudin CM. Selective tropism of Seneca Valley virus for variant subtype small cell lung cancer. J Natl. Cancer Inst. 2013; 105:1059–1065. [PubMed: 23739064]
41. Barretina J, Caponigro G, Stransky N, Venkatesan K, Margolin AA, Kim S, Wilson CJ, Lehár J, Kryukov GV, Sonkin D, Reddy A, Liu M, Murray L, Berger MF, Monahan JE, Morais P, Meltzer J, Korejwa A, Jané-Valbuena J, Mapa FA, Thibault J, Bric-Furlong E, Raman P, Shipway A, Engels IH, Cheng J, Yu GK, Yu J, Aspesi P Jr, de Silva M, Jagtap K, Jones MD, Wang L, Hatton C, Palescandolo E, Gupta S, Mahan S, Sougnez C, Onofrio RC, Liefeld T, MacConaill L, Winckler W, Reich M, Li N, Mesirov JP, Gabriel SB, Getz G, Ardlie K, Chan V, Myer VE, Weber BL, Porter J, Warmuth M, Finan P, Harris JL, Meyerson M, Golub TR, Morrissey MP, Sellers WR, Schlegel R, Garraway LA. The Cancer Cell Line Encyclopedia enables predictive modeling of anticancer drug sensitivity. Nature. 2012; 483:603–607. [PubMed: 22460905]
42. Kosari F, Ida CM, Aubry M-C, Yang L, Kovtun IV, Klein JL, Li Y, Erdogan S, Tomaszek SC, Murphy SJ, Bolette LC, Kolbert CP, Yang P, Wigle DA, Vasmatzis G. ASCL1 and RET expression defines a clinically relevant subgroup of lung adenocarcinoma characterized by neuroendocrine differentiation. Oncogene. 2014; 33:3776–3783. [PubMed: 24037524]
43. Mairhofer M, Steiner M, Salzer U, Prohaska R. Stomatin-like protein-1 interacts with stomatin and is targeted to late endosomes. J Biol. Chem. 2009; 284:29218–29229. [PubMed: 19696025]
44. Choi KY, Swierczewska M, Lee S, Chen X. Protease-activated drug development. Theranostics. 2012; 2:156–178. [PubMed: 22400063]
45. Dubowchik GM, Firestone RA, Padilla L, Willner D, Hofstead SJ, Mosure K, Knipe JO, Lasch SJ, Trail PA. Cathepsin B-labile dipeptide linkers for lysosomal release of doxorubicin from internalizing immunoconjugates: Model studies of enzymatic drug release and antigen-specific in vitro anticancer activity. Bioconjug. Chem. 2002; 13:855–869. [PubMed: 12121142]
46. Puzanov I, Lee W, Chen AP, Calcutt MW, Hachey DL, Vermeulen WL, Spanswick VJ, Liao C-Y, Hartley JA, Berlin JD, Rothenberg ML. Phase I pharmacokinetic and pharmacodynamic study of SJG-136, a novel DNA sequence selective minor groove cross-linking agent, in advanced solid tumors. Clin. Cancer Res. 2011; 17:3794–3802. [PubMed: 21346148]
47. Pagliarini R, Shao W, Sellers WR. Oncogene addiction: Pathways of therapeutic response, resistance, and road maps toward a cure. EMBO Rep. 2015; 16:280–296. [PubMed: 25680965]
48. Osada H, Tatematsu Y, Yatabe Y, Horio Y, Takahashi T. *ASH1* gene is a specific therapeutic target for lung cancers with neuroendocrine features. Cancer Res. 2005; 65:10680–10685. [PubMed: 16322211]
49. Garraway LA, Sellers WR. Lineage dependency and lineage-survival oncogenes in human cancer. Nat. Rev. Cancer. 2006; 6:593–602. [PubMed: 16862190]
50. Hartley JA, Spanswick VJ, Brooks N, Clingen PH, McHugh PJ, Hochhauser D, Pedley RB, Kelland LR, Alley MC, Schultz R, Hollingshead MG, Schweikart KM, Tomaszewski JE, Sausville

EA, Gregson SJ, Howard PW, Thurston DE. SJG-136 (NSC 694501), a novel rationally designed DNA minor groove interstrand cross-linking agent with potent and broad spectrum antitumor activity: Part 1: Cellular pharmacology, in vitro and initial in vivo antitumor activity. Cancer Res. 2004; 64:6693–6699. [PubMed: 15374986]

51. Clingen PH, De Silva IU, McHugh PJ, Ghadessy FJ, Tilby MJ, Thurston DE, Hartley JA. The XPF-ERCC1 endonuclease and homologous recombination contribute to the repair of minor groove DNA interstrand crosslinks in mammalian cells produced by the pyrrolo[2,1-c] [1,4]benzodiazepine dimer SJG-136. Nucleic Acids Res. 2005; 33:3283–3291. [PubMed: 15944449]
52. Ito T, Udaka N, Yazawa T, Okudela K, Hayashi H, Sudo T, Guillemot F, Kageyama R, Kitamura H. Basic helix-loop-helix transcription factors regulate the neuroendocrine differentiation of fetal mouse pulmonary epithelium. Development. 2000; 127:3913–3921. [PubMed: 10952889]
53. Bolstad BM, Irizarry RA, Åstrand M, Speed TP. A comparison of normalization methods for high density oligonucleotide array data based on variance and bias. Bioinformatics. 2003; 19:185–193. [PubMed: 12538238]

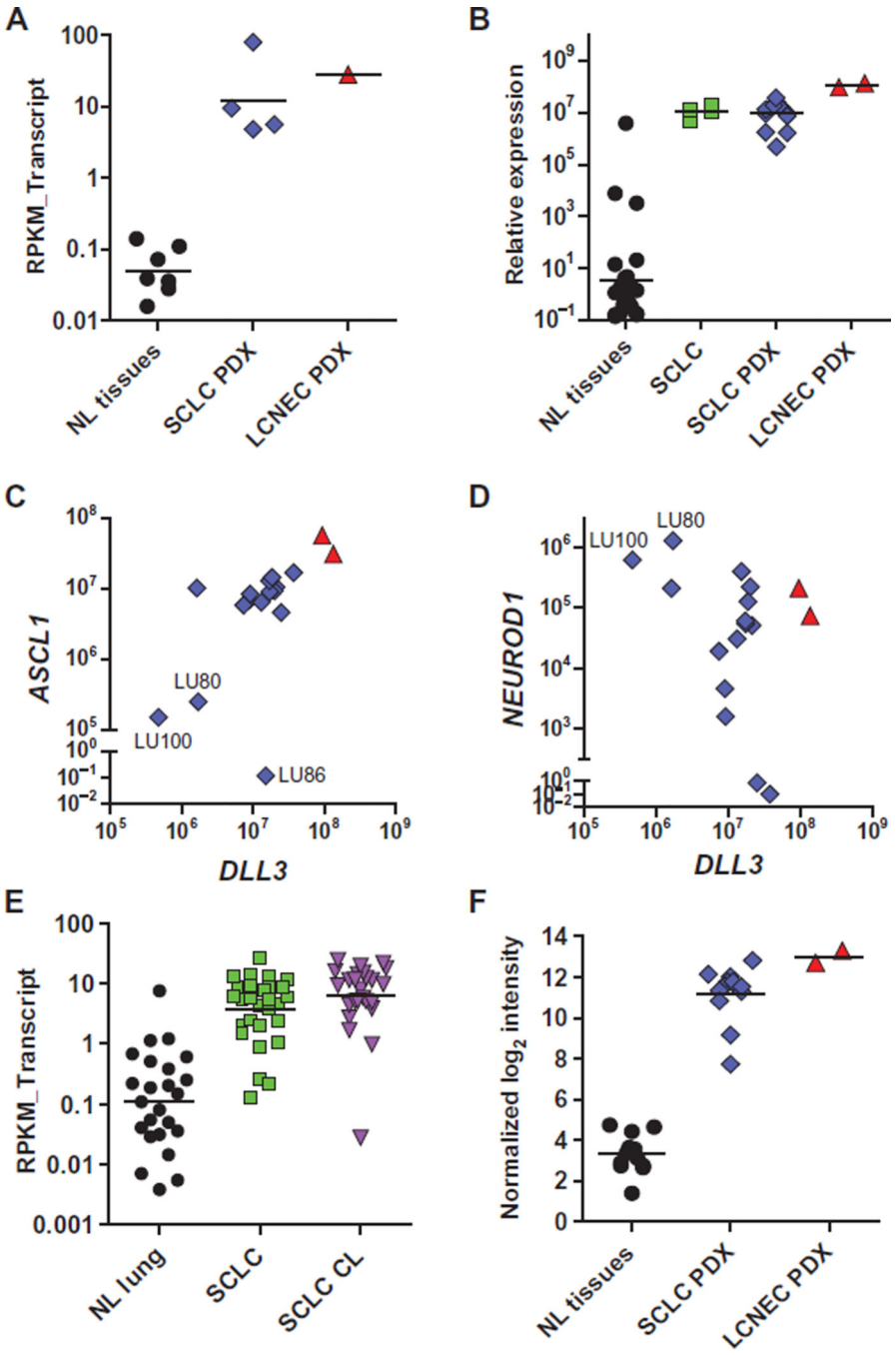

Fig. 1. Elevated expression of *DLL3* mRNA in SCLC

(**A**) *DLL3* transcripts conveyed as reads per kilobase per million reads mapped to annotated exons (RPKM_Transcript) in normal tissues (NL tissues) and SCLC and LCNEC PDXs. (**B**) Relative expression of *DLL3* in NL tissues, primary SCLC biopsy specimens (SCLC), and SCLC and LCNEC PDX, as measured by quantitative PCR. (**C** and **D**) Relative expression of *ASCL1* (C) and *NEUROD1* (D) versus *DLL3* in SCLC (blue diamond) and LCNEC (red triangle) PDX, as measured by quantitative PCR. (**E**) *DLL3* transcripts (RPKM_Transcript) in normal lung, primary SCLC tumors, and SCLC cell lines (CL). (**F**) Quantile normalized

$\log_2$ intensity values of *DLL3* mRNA in NL tissues and PDX lines assessed by microarray. Horizontal bars represent the geometric mean. Normal tissues included in each expression metric are detailed in table S1.

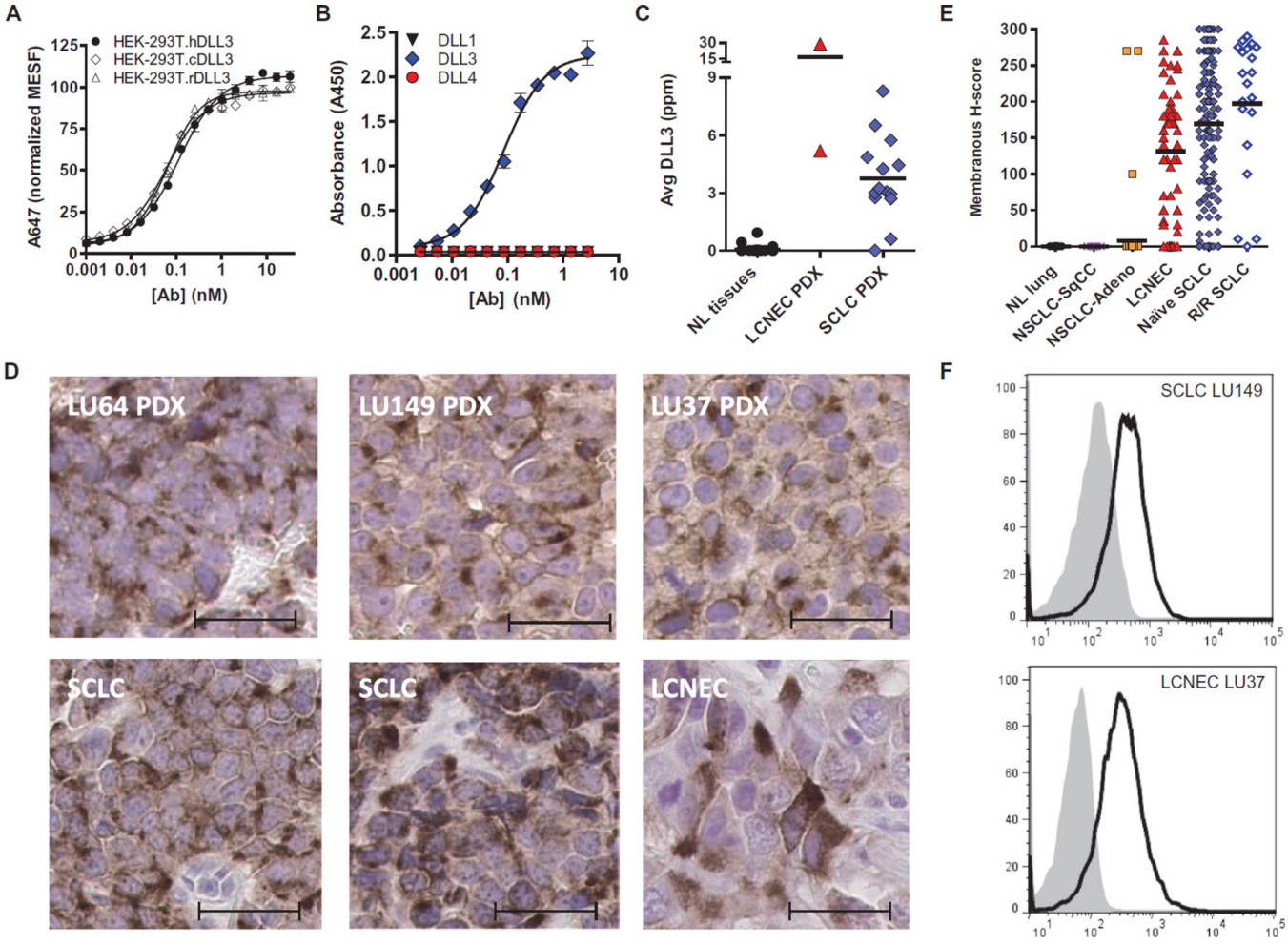

Fig. 2. Characterization of DLL3-specific and species cross-reactive monoclonal antibodies

(**A**) SC16 shows equivalent binding to human, cyno, and rat DLL3 expressed on the surface of HEK-293T cells. (**B**) SC16 reacts only with DLL3 and not related family members DLL1 or DLL4. (**C**) DLL3 protein was detected in SCLC and LCNEC PDX by ELISA. Horizontal bars represent the mean. Normal tissue samples and the amounts of DLL3 protein detected are detailed in table S1. (**D**) IHC of two SCLC (LU64, *H*-score = 96; LU149, *H*-score = 134) and one LCNEC (LU37, *H*-score = 147) PDX, as well as primary SCLC (*H*-score = 170 and 200) and LCNEC (*H*-score = 160) tumors. Scale bars, 20 μm. (**E**) DLL3 membrane expression as measured by IHC in normal lung tissue and primary tumors including lung squamous cell (NSCLC-SqCC), lung adenocarcinoma (NSCLC-Adeno), LCNEC, and naïve and recurrent/refractory (R/R) SCLC. Horizontal bars represent the mean. (**F**) Surface DLL3 expression on SCLC LU149 and LCNEC LU37 PDX tumor cells assessed by flow cytometry with phycoerythrin (PE)–conjugated anti-DLL3 (black line) or IgG1 isotype control (gray-filled) antibodies. MESF, mean equivalents of soluble fluorescein.

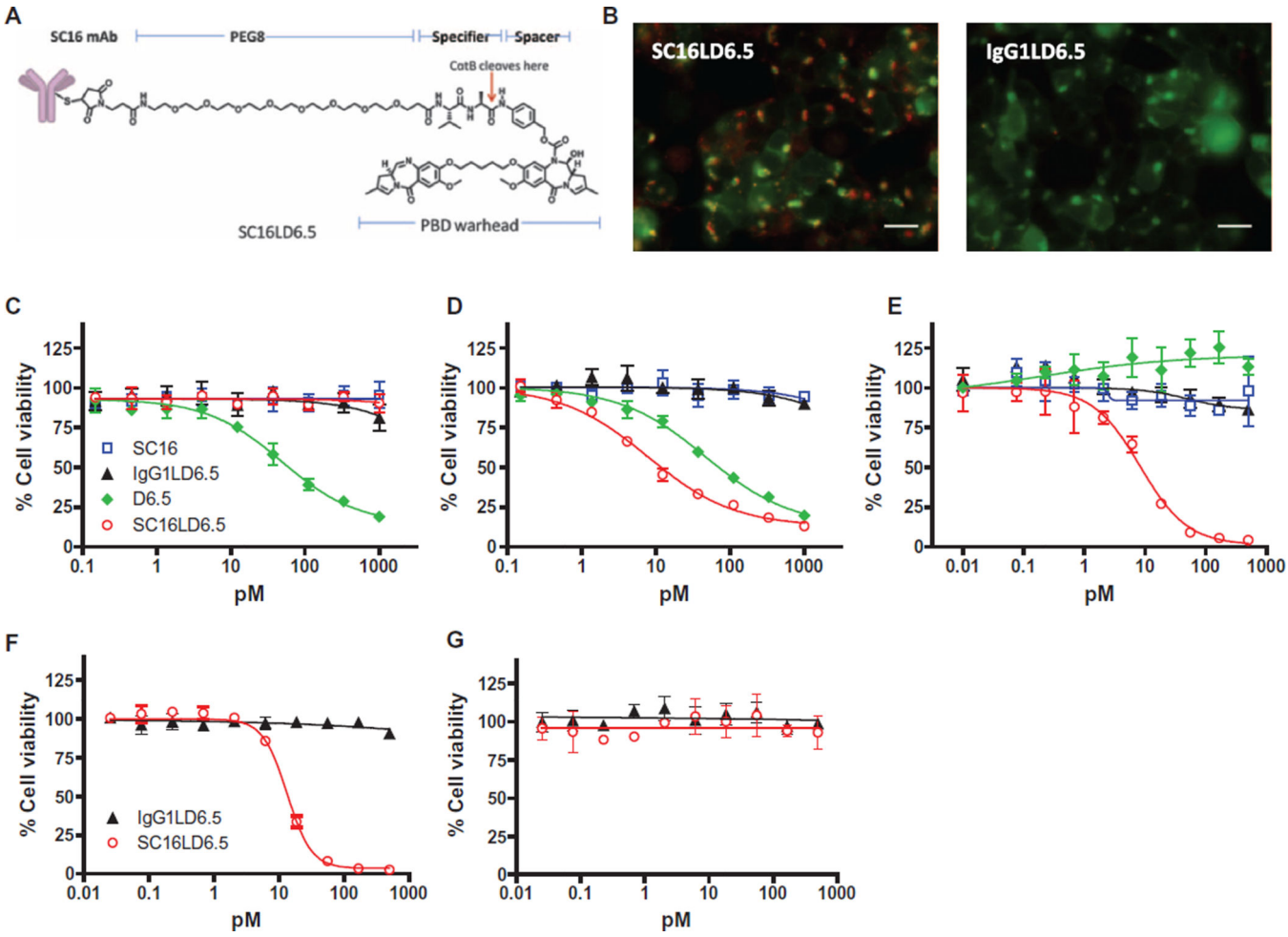

Fig. 3. Characterization of DLL3-mediated internalization and cytotoxicity

(**A**) Schematic of SC16LD6.5. (**B**) Demonstration of SC16LD6.5 and IgG1LD6.5 localization (red) in HEK-293T.hDLL3 cells engineered to express red fluorescent protein (RFP)–SLP-1 (false color displayed as green) in late endosomes. Colocalization is indicated by yellow/orange. Scale bars, 25 μm. (**C** to **G**) In vitro cytotoxicity of SC16, IgG1LD6.5, D6.5, and SC16LD6.5 upon incubation with (C) HEK-293T, (D) HEK-293T. hDLL3, (E) LU64 PDX, (F) LU37 PDX expressing endogenous DLL3, or (G) LU37 PDX lacking DLL3 expression (LU37.D3hp) after shRNA-mediated knockdown. mAb, monoclonal antibody.

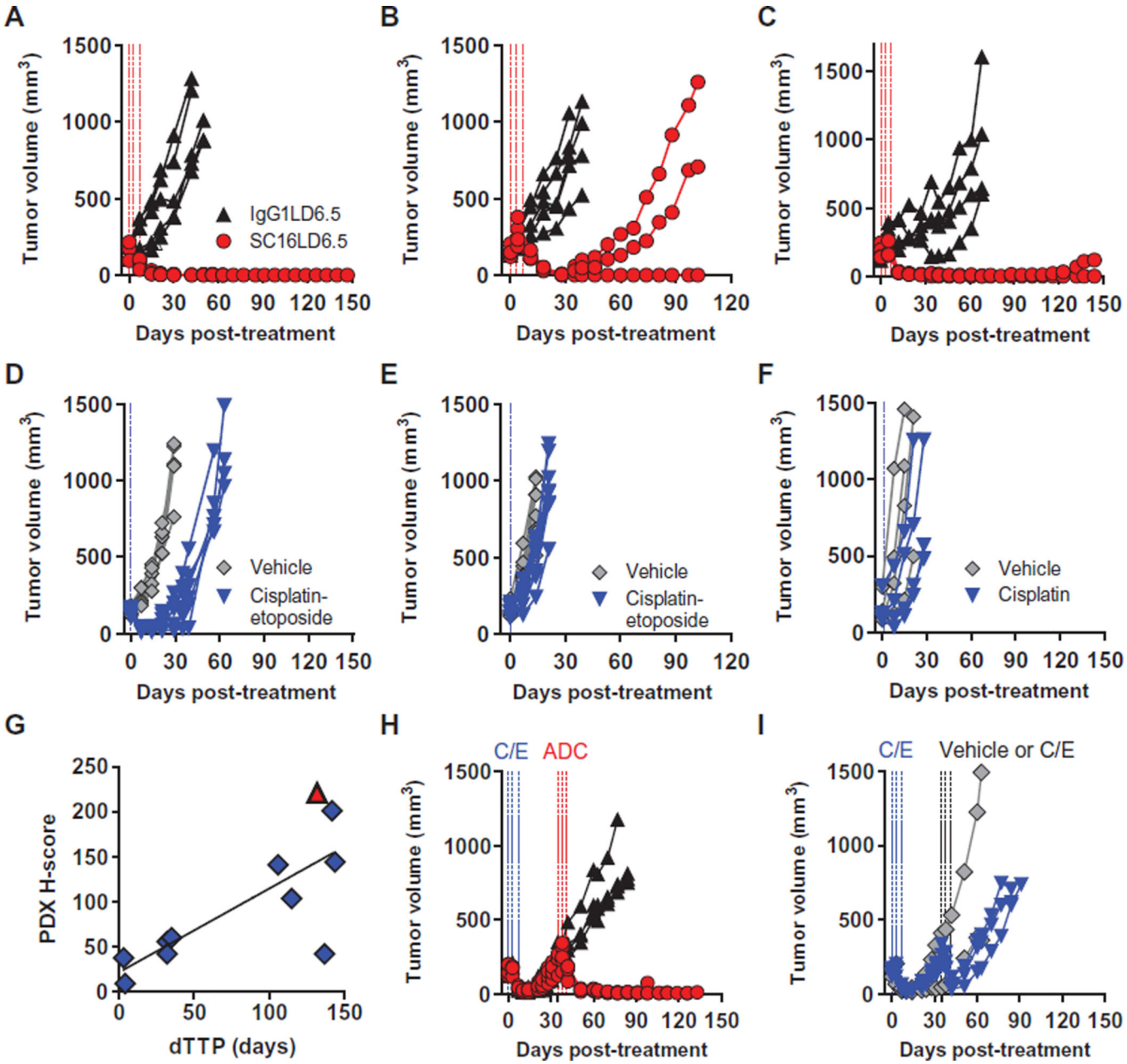

Fig. 4. Demonstration of in vivo efficacy with SC16LD6.5

(**A** to **F**) Mice bearing SCLC LU64 (A and D), SCLC LU86 (B and E), or LCNEC LU37 (C and F) PDX tumors were treated with IgG1LD6.5 or SC16LD6.5 (1 mg/kg) (A to C) on a Q4D×3 regimen, or vehicle (saline) or SOC chemotherapy (D to F). (**G**) DLL3 surface expression quantified by IHC (*H*-score) correlated with dTTP in 10 SCLC and 1 LCNEC PDX model. (**H** and **I**) Mice bearing SCLC LU64 PDX tumors were treated with C/E and, upon tumor recurrence (35 days after initial C/E treatment), were randomized and treated again either with (H) IgG1LD6.5 or SC16LD6.5 (1 mg/kg) on a Q4D×3 regimen or with (I) vehicle or C/E.

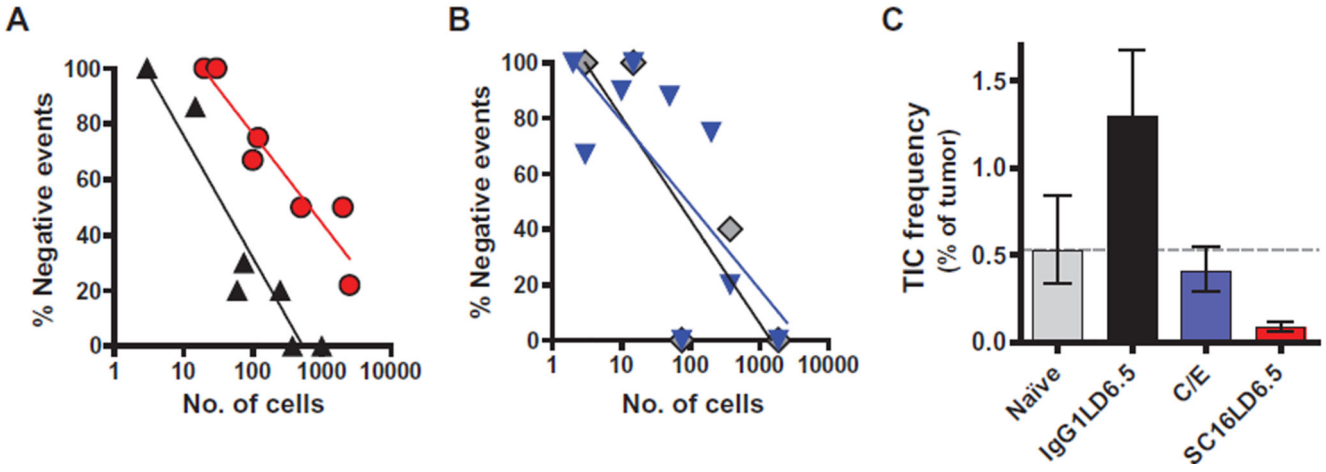

Fig. 5. Elimination of TIC by SC16LD6.5

(**A**) The frequency of no tumor growth after serial transplantation of SCLC LU64 PDX tumor cells in limiting dilutions is shown for IgGLD6.5 (black triangles) and SC16LD6.5 (red circles) cohorts. (**B**) The frequency of no tumor growth after serial transplantation of SCLC LU64 PDX tumor cells in limiting dilutions is shown for the naïve (gray diamonds) and C/E (blue triangles) cohorts. (**C**) The frequency of TICs was estimated by Poisson distribution statistics using tumor growth frequencies within each cohort.

Table 1

In vivo efficacy of SC16LD6.5 and TIC frequency in SCLC and LCNEC PDX

%TGI, percent tumor growth inhibition; Q4D×3, once every 4 days for a total of three doses; N.D., not determined; SD, single dose. SOC for SCLC: cisplatin (5 mg/kg) SD on day 0 and etoposide (8 mg/kg) on days 0, 1, and 2; LCNEC: cisplatin (5 mg/kg) SD. AJCC, American Joint Committee on Cancer.

Tumor type	PDX	AJCC stage	Untreated TIC frequency*	SOC	DLL3 protein (ng/mg)	SC16LD6.5		
				%TGI (dTTP; days)		Dose level (mg/kg)	Regimen	%TGI (dTTP; days)
SCLC	LU64	IV	1:189	86 (18)	4.25	1	Q4D×3	100 (133)
	LU73	IIIa	1:136	86 (28)	2.77	1	Q4D×3	77 (32)
	LU80	IV	1:143	82 (14)	0.60	1	Q4D×3	55 (4)
	LU86	IV	1:31	39 (0)	3.05	1	Q4D×3	80 (32)
	LU95	IV	1:60	56 (14)	6.52	1	Q4D×3	95 (115)
	LU100	Ia	1:166	100 (64)	0.001	1	Q4D×3	96 (3)
	LU117	IV	1:388	99 (25)	2.95	1	Q4D×3	99 (137)
	LU124	IIIb	1:271	85 (14)	3.23	1	Q4D×3	72 (35)
	LU129	IV	N.D.	84 (32)	N.D.	1	Q4D×3	95 (106)
	LU149	IV	1:207	93 (21)	2.71	1	Q4D×3	99 (142)†
Mean				81 (23)				87 (74)
SEM				6 (5)				5 (18)
Median				86 (17)				95 (71)
LCNEC	LU37	IIb	1:16	60 (4)	5.19	1	Q4D×3	97 (132)
	LU240	IIb	1:31	27 (0)	28.57	2	SD	95 (42)
Mean				44 (2)				96 (87)
SEM				17 (2)				1 (45)
Median				44 (2)				96 (87)

*Determined by implanting various cell doses (2 to 1000 cells) of dissociated cells from passage 2 to 5 PDX into mice.

†IgG1.LD6.5 data not available; dTTP value represents TTP.